JOURNAL OF GEOPHYSICAL RESEARCH, VOL. 102, NO. B10, PAGES 22,799–22,813, OCTOBER 10, 1997

Regional waveform calibration in the Pamir-Hindu Kush region

Lupei Zhu and Donald V. Helmberger

Seismological Laboratory, California Institute of Technology, Pasadena

Chandan K. Saikia and Bradley B. Woods

Woodward-Clyde Federal Services, Pasadena, California

Abstract. Twelve moderate-magnitude earthquakes (m_b 4-5.5) in the Pamir-Hindu Kush region are investigated to determine their focal mechanisms and to relocate them using their regional waveform records at two broadband arrays, the Kyrgyzstan Regional Network (KNET), and the 1992 Pakistan Himalayas seismic experiment array (PAKH) in northern Pakistan. We use the "cut-and-paste" source estimation technique to invert the whole broadband waveforms for mechanisms and depths, assuming a one-dimensional velocity model developed for the adjacent Tibetan plateau. For several large events the source mechanisms obtained agree with those available from the Harvard centroid moment tensor (CMT) solutions. An advantage of using regional broadband waveforms is that focal depths can be better constrained either from amplitude ratios of Pnl to surface waves for crustal events or from time separation between the direct P and the shear-coupled P wave ($sPn + sPmP$) for mantle events. All the crustal events are relocated at shallower depths compared with their International Seismological Centre bulletin or Harvard CMT depths. After the focal depths are established, the events are then relocated horizontally using their first-arrival times. Only minor offsets in epicentral location are found for all mantle events and the bigger crustal events, while rather large offsets (up to 30 km) occur for the smaller crustal events. We also tested the performance of waveform inversion using only two broadband stations, one from the KNET array in the north of the region and one from the PAKH array in the south. We found that this geometry is adequate for determining focal depths and mechanisms of moderate size earthquakes in the Pamir-Hindu Kush region.

1. Introduction

Recent advances in real-time seismic data acquisition, computation power, and source estimation techniques have greatly improved our ability to analyze seismic sources. Currently, earthquakes of magnitude larger than 5.5 anywhere on the globe can be processed semi-automatically or automatically to determine the locations and source mechanisms using their long-period surface waveforms and/or body waveforms [*Dziewonski and Woodhouse*, 1983; *Sipkin*, 1986; *Kawakatsu*, 1995; *Polet and Kanamori*, 1995]. In order to lower the magnitude threshold it is inevitable that one has to rely on seismic records at regional distances (less than 1000 km). However, although the number of digital seismic stations has increased dramatically in recent years, there are regions in the world where only one or two digital stations are available within these distances. This is especially true for some geographically remote but tectonically highly interesting regions such as the Pamir-Hindu Kush.

Located at the western end of the India-Eurasia continental collision zone, the Pamir-Hindu Kush region has been for many years a focus of geological and geophysical investigations. It has a well-known intermediate-depth seismic zone which is apparently not associated with current oceanic subductions (Plate 1). Whether this intensive seismic zone is produced by a remnant of oceanic slab or subducted continental lithosphere is still under debate [*Billington et al.*, 1977; *Mellors et al.*, 1995]. Understanding the accurate spatial distribution of earthquakes in the region and their source mechanisms can be crucial in resolving the actual geometry of the slab and its stress state.

In this study we will establish the ability of two permanent Incorporated Research Institutions for Seismology (IRIS) stations, NIL in Pakistan and AAK in Kyrgyzstan (see Plate 1) to locate and determine source characteristics of events in the Pamir-Hindu Kush region. AAK is one of the stations of Kyrgyzstan Regional

Paper number 97JB01855.
0148-0227/97/97JB-01855$09.00

Network (KNET). During the 1922 Pakistan Himalayas passive source broadband seismic experiment (PAKH) [see *Sandvol et al.*, 1994], a temporary seismic array was deployed in northern Pakistan, which is very close to NIL. To calibrate the paths of events to AAK and NIL, we selected 12 moderate-magnitude events (m_b 4-5.5, see Table 1) which occurred in the time window of the PAKH deployment. Using the two arrays, we determine the source parameters and depths of these events from their broadband waveforms followed by a relocation using the first-arrival times. Then, we repeat the same process using only two stations. Since NIL was not installed in this time period, the closest station from the PAKH array, SBRA, was used as a surrogate for it along with AAK when performing the two-station analysis. We found that they gave results compatible with those of two arrays. Thus future events in the Pamir-Hindu Kush region can be processed routinely using stations AAK and NIL to provide a more uniform and well-constrained data set on the earthquake distribution and focal mechanisms for this important region.

2. Regional Seismicity

The Pamir-Hindu Kush has intensive seismic activity ranging from a shallow depth all the way down to a 350 km depth. The distribution of shallow earthquakes is generally broad and diffusive except in the northern margin of the Pamir where earthquakes are concentrated more or less along a narrow belt (Plate 1). In contrast, most intermediate-depth events occur in a relatively narrow SW-NE zone. Several detailed studies have shown that this intermediate-depth seismic zone is composed of two separate segments with a 50 km gap between them [*Billington et al.*, 1977; *Roecker et al.*, 1980; *Chatelain et al.*, 1980]. The eastern segment strikes NE beneath the Pamir with the seismicity terminating at a depth of about 200 km. The E-W oriented western segment beneath the northern end of the Hindu Kush range extends deeper and is more active. Correspondingly, two narrow Wadati-Benioff zones were defined, with the one under the Hindu Kush dipping to the north and the other, under the Pamir, dipping to the southeast (Figure 1). These studies suggest dual interpretations of either a single contorted slab or two distinct slabs with opposing subduction directions [*Billington et al.*, 1977; *Roecker et al.*, 1980; *Burtman and Molnar*, 1993; *Fan et al.*, 1994]. The concentrated shallow seismic zone along the northern margin of the Pamir may be the intersection of the southeast dipping Pamir seismic zone on the surface [*Hamburger et al.*, 1992; *Fan et al.*, 1994]. However the aseismic gap between intermediate-depth and shallow seismic zones makes it difficult to correlate them (Figure 1c). There is no obvious crustal seismicity associated with the Hindu-Kush segment. In addition, at depths of about 150 to 170 km, there is an obscure minimum in the seismic activity and a sudden steepening of the dip angle of the Wadati-Benioff zone (Figure 1a and Figure 1b).

It is worth pointing out that despite the high level of seismic activity in the region, most earthquakes are moderate size and therefore are not recorded well at teleseismic distances. Comparison of the preliminary determination of epicenters (PDE) using the global network with a regional bulletin, compiled using several IRIS networks in central Asia and Global Seismic Network (GSN) and Chinese Digital Seismic Network (CDSN) data, shows that the PDE is only complete down to magnitude 4.5, and its location error is an order of magnitude larger than the regional bulletin [*Harvey*, 1996]. Therefore it is of great significance to utilize regional distance waveform records to locate earthquakes.

3. Method and Regional Velocity Model

A detailed description of our source estimation technique using broadband regional waveforms can be found in *Zhao and Helmberger* [1994] and *Zhu and Helmberger* [1996b]. We will only give a brief summary here. Usually, waveforms at regional distances are complicated and contain detailed information about the source rupture and the Earth structure through which they propagate. For crustal events beyond the distance range of 200-300 km the first 1-2 min of waveform is called *Pnl*,

Table 1. Event Locations From International Seismological Centre (ISC) Catalog

Event	Date	Origin Time, UT	Location	h, km	m_b
276	Oct. 02, 1992	1438:46.4	38.08N/73.12E	139	4.6
289a	Oct. 15, 1992	0242:06.7	39.24N/72.80E	16	4.5
289b	Oct. 15, 1992	1942:13.8	38.20N/74.44E	157	4.4
307	Nov. 02, 1992	0452:55.2	37.28N/72.06E	148	4.7
311a	Nov. 06, 1992	0721:56.0	41.09N/72.50E	21	5.1
311b	Nov. 06, 1992	1758:39.0	34.87N/69.15E	25	4.5
313	Nov. 08, 1992	2050:07.0	38.70N/69.82E	12	5.3
317	Nov. 12, 1992	2041:05.2	36.45N/70.87E	204	5.5
322	Nov. 17, 1992	0238:50.7	33.83N/67.53E	35	5.1
328	Nov. 23, 1992	2311:06.9	38.57N/72.65E	43	5.6
339	Dec. 04, 1992	1136:35.5	37.79N/72.21E	114	5.8
341	Dec. 06, 1992	0344:29.3	37.79N/72.19E	122	5.5

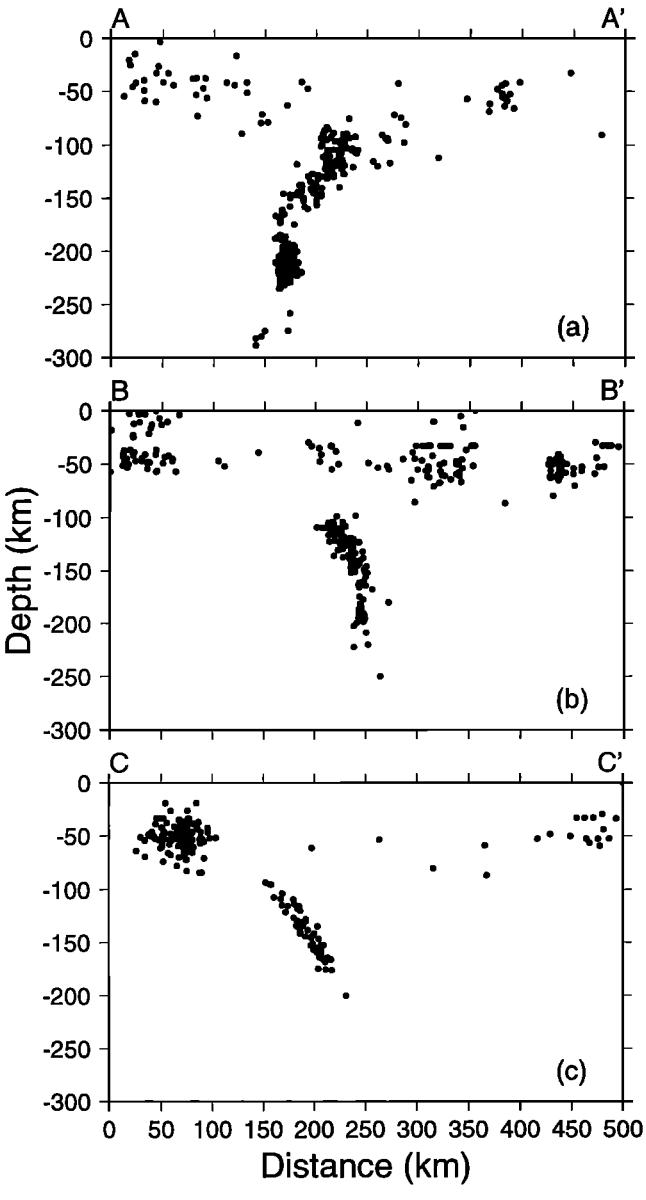

Figure 1. Three cross sections of the ISC hypocenters (locations shown in Plate 1). These cross sections have horizontal widths of 100 km and are oriented so they are perpendicular to the strike of the Wadati-Benioff zone and intersect the Hindu-Kush segment (profile AA'), middle Pamir segment (BB'), and eastern end of the Pamir segment (CC').

which consists of the P arrival (Pn) followed by the crust-trapped P-SV multiple conversions (PL). The large-amplitude surface waves (Rayleigh/Love) appear later in the record. There are two issues which make a source estimation using the whole waveform difficult: First, the whole-waveform inversion is mainly controlled by the surface waves because of their large amplitude. But *Pnl* is very useful for source estimation because it is more stable and insensitive to velocity structure [*Helmberger and Engen*, 1980], and the amplitude ratio between *Pnl* and surface waves is a good discriminant of source depth. Second, these two portions of waveform sample different parts of the Earth structure and thus require different adjustments of the velocity model used. To overcome these difficulties, *Zhao and Helmberger* [1994] developed a cut-and-paste (CAP) source estimation technique which breaks the whole waveform into the *Pnl* and surface wave segments and inverts them independently. When comparing each segment with synthetics, it allows time shifts between the two to get maximum alignment. This relaxation of timing proves to be quite helpful when only imperfect velocity model and inaccurate event locations are available at the start.

Recently, we improved the CAP method by redefining the waveform misfit error to preserve amplitude information of waveforms, so focal depth and source mechanism can be better constrained [*Zhu and Helmberger*, 1996b]. The misfit error between a segment of observed waveform $u(t)$ and synthetics $s(t)$ is defined as

$$e = \| \left(\frac{r}{r_0}\right)^p \| \quad \| u(t) - s(t) \|,$$

here p is a scaling factor to give the record at distance r the same weight as that at reference distance r_0 (100 km usually). If we assume a spherical geometrical spreading for body waves and cylindrical geometrical spreading for surface waves, an appropriate choice of p would be 1 for *Pnl* waves and 0.5 for surface waves. It can also be adjusted corresponding to the actual amplitude decays of these phases after a certain amount of data has been accumulated for a particular area.

The misfit error for the whole waveform is the summation of the two parts:

$$e_{\text{total}} = w_{Pnl}\, e_{Pnl} + e_{\text{surf}},$$

a static weighting factor w_{Pnl} is introduced to balance the contributions from *Pnl* and surface waves because usually the amplitude of surface waves is 2-3 times larger even after the distance decay correction. We also want to emphasize the *Pnl* because of its insensitivity to structural lateral variations. In this study we use a w_{Pnl} of 4.

A solution of source mechanism and depth is obtained by a grid search through the whole source parameter space, thus eliminating the need of calculating differential seismograms [*Zhao and Helmberger*, 1994]. Another advantage is that the resolution of the solution can be estimated by examining the misfit errors in the vicinity of the minimum ("best solution").

The velocity model used for the study area is listed in Table 2. This simple one-dimensional (1-D) velocity model was developed from modeling regional broadband waveforms and teleseismic receiver functions in the adjacent Tibet plateau [*Zhu et al.*, 1993; *Zhu and Helmberger*, 1994]. The model has a crustal thickness of 64 km with an average P velocity of 6.2 km $s^{-1}$and S velocity of 3.5 km s^{-1}. The velocity structure of the Pamir-Hindu Kush has been studied by several re-

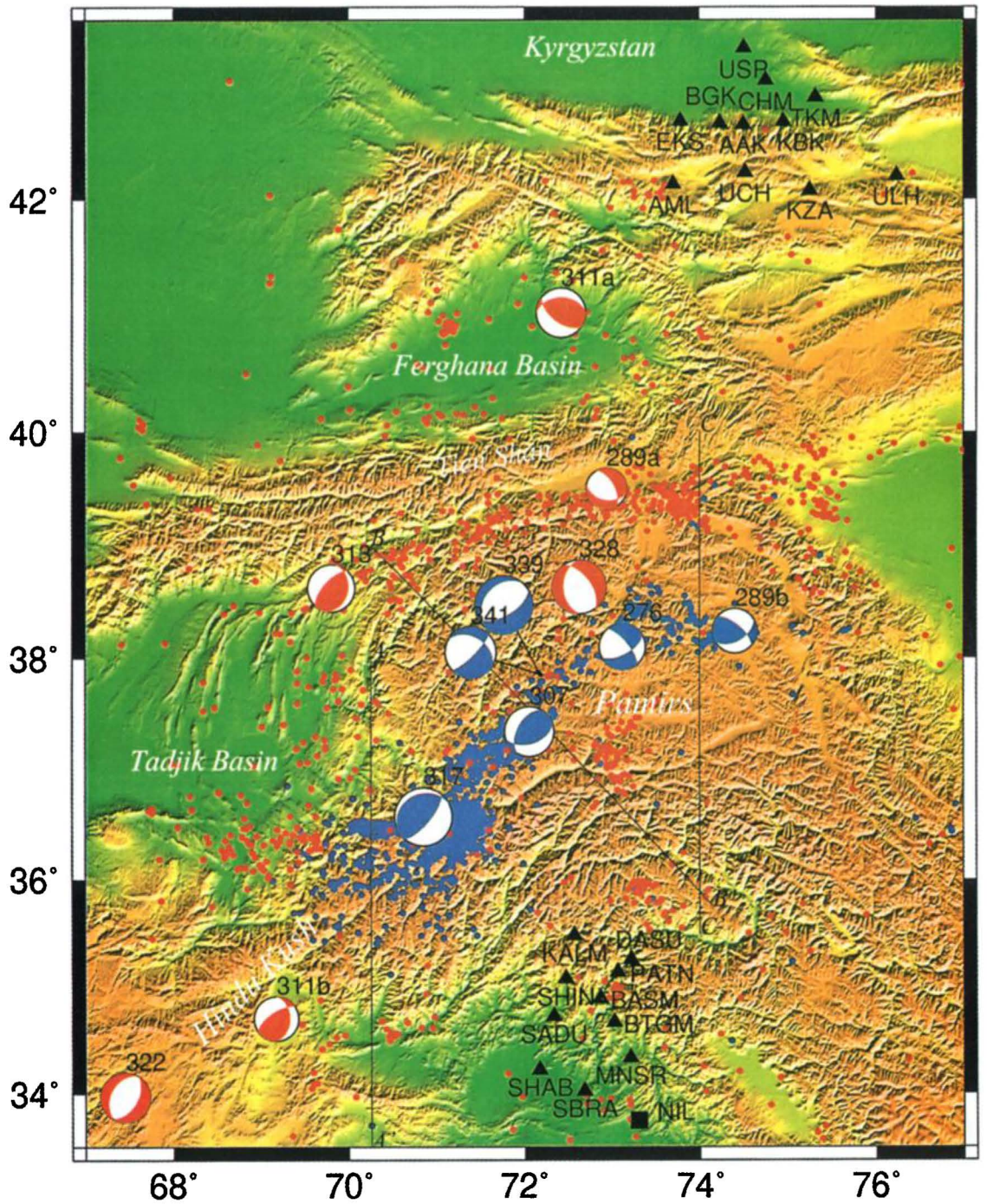

Plate 1. Map of the Pamir-Hindu Kush region showing topography (green tone indicates elevation below 2 km) and the stations of the Kyrgyzstan Regional Network (KNET) and the 1992 Pakistan Himalayas seismic experiment (PAKH) arrays (triangles). Blue and red dots are intermediate-depth ($\geq$ 70 km) and crustal events respectively, as reported by the International Seismological Centre (ISC) between 1964 and 1993. These events all have more than 20 stations reported, and the location errors are less than 10 km as listed in the catalog. The focal spheres represent the waveform inversion results of the 12 events in this study. The numbers next to the spheres are the Julian days of events used as event identifications.

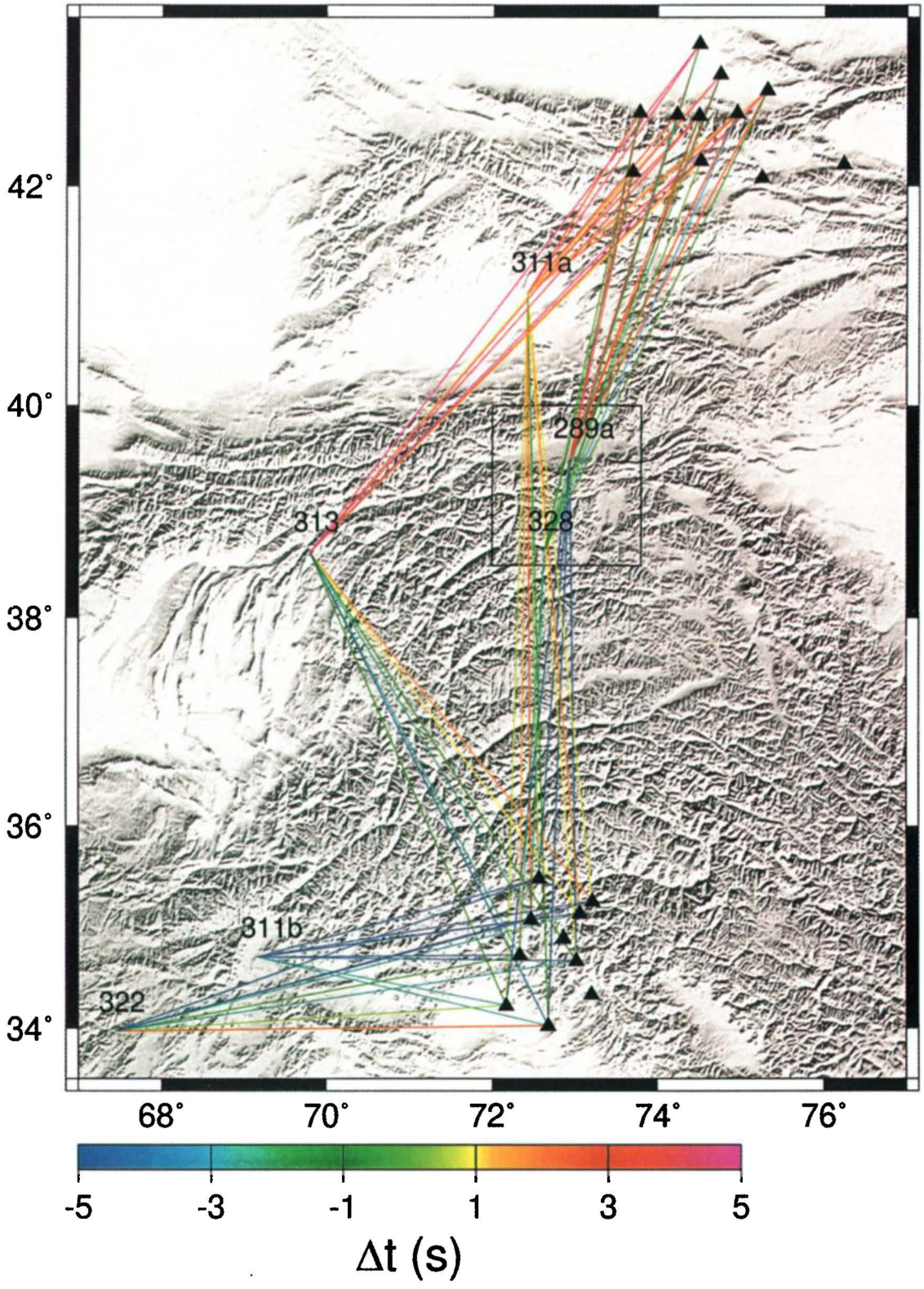

Plate 2. Time shifts of Love waves as produced by the waveform inversion. Positive shifts indicate later Love wave arrivals with respect to the 1-D model. The insert box shows the location of Figure 8.

Table 2. One-Dimensional Velocity Model of the Study Area

Layer	Thickness, km	V_p, km s^{-1}	V_s, km s^{-1}
1	4	4.70	2.70
2	60	6.20	3.50
3	–	8.14	4.70

searchers. For example, using travel times of local events, *Roecker* [1982] derived a one-layer (70 km thick; Vp, 6.4 km s^{-1}; Vs, 3.7 km s^{-1}) crustal model for this region. *Zhao and Helmberger* [1993] developed a four-layer model with Moho at 65 km by modeling regional waveforms from intermediate-depth events recorded at station GAR. The gross features of our model are very similar to these models, except our crustal velocities are slightly lower. Our model is also consistent with the result of the seismic refraction profile transversing the study area approximately along 70°E meridian [*Beloussov et al.*, 1980]. This profile also shows lateral variation of crustal structure: The crustal thickness increases from 50-55 km in the Ferghana basin, Tien Shan, to 70-75 km in the northern Pamir, and varies between 60 and 65 km for the central and southern Pamir, Karakorum, and inner Himalayas [*Beloussov et al.*, 1980]. Since our inversion method allows time

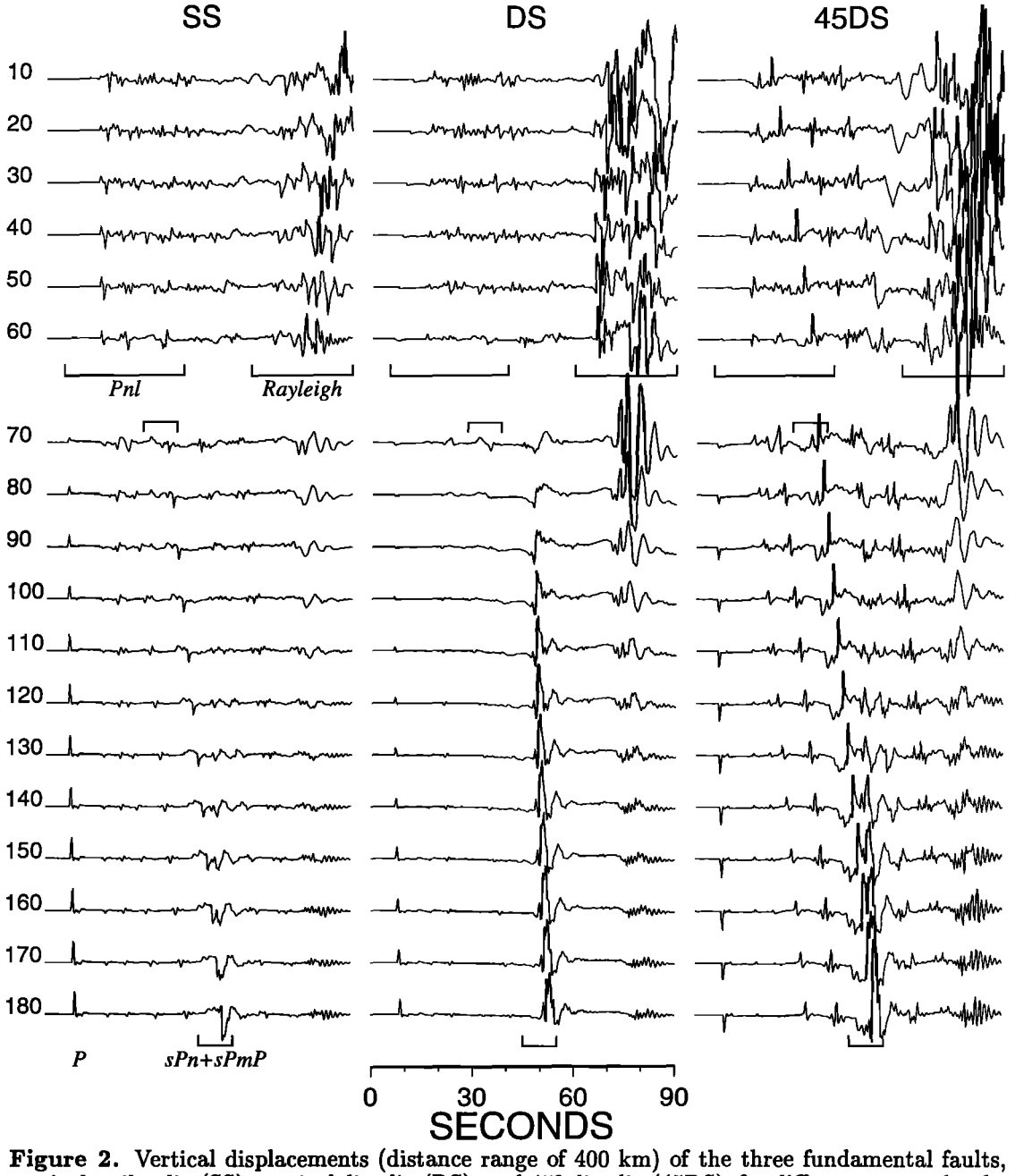

Figure 2. Vertical displacements (distance range of 400 km) of the three fundamental faults, vertical strike-slip (SS), vertical dip slip (DS), and 45° dip slip (45DS), for different source depths (given by numbers on the left in kilometers). The Moho is at a depth of 64 km. The amplitudes for mantle events have been multiplied by 2 to account for the velocity and density jumps across the Moho. Several phases discussed in the text are labeled.

shifts between observed waveform and synthetics, most of the discrepancies of the 1-D velocity model from the true Earth model can be absorbed by the time shift term. We have tested different modifications of our two-layer 1-D model, including increasing velocities in the mid-lower crust and replacing the sharp Moho discontinuity with a transition zone. Essentially, the same inversion results are obtained [*Saikia et al.*, 1996].

The full responses of the 1-D model for various source depths and distance ranges are computed using the frequency-wavenumber (F-K)double integration algorithm [*Wang and Herrmann*, 1980; *Saikia*, 1994]. As an example, the vertical displacements of the three fundamental faults at different depths are displayed in Figure 2. The corresponding tangential components are quite simple and have been presented in *Zhu and Helmberger* [1996a]. For crustal events the amplitudes of surface waves are very large for shallow events, so the amplitude ratio between surface waves to *Pnl* is quite diagnostic in determining focal depth. As the source moves into the mantle, the high-frequency signals trapped by the crustal waveguide disappear. The waveforms become increasingly simple as the focal depth increases, essentially reducing to just a P wave and S wave, as shown in the figure. However, there is still important information about polarity and relative strengths of the phases. We will discuss this in detail in the next section.

4. Focal Depths and Source Mechanisms

The velocity records of the 12 events at the KNET and PAKH arrays were converted into displacements by removing the instrument responses and band passed between 5 and 100 s. These waveforms were then inverted for the source mechanisms and depths using the CAP method. The parameter space of source orientation is grid searched at 10° intervals in strike, dip, and rake. Source depth is searched at 5 km spacing for crustal events and 10 km spacing for subcrustal events. The results are listed in Table 3. The lower hemisphere projections of the corresponding source mechanisms are plotted in Plate 1.

Among the 12 events the 5 largest ones have Harvard CMT solutions available in the International Seismological Centre (ISC) bulletin. These solutions are also listed in Table 3. As one can see, our focal mechanisms agree with the Harvard ones. The differences between source orientation are within 10° to 15° for most events. The largest difference is for event 311a. Although both give a similar thrust mechanism, their strikes and rakes differ by about 50°. Figure 3 shows the waveforms of KNET stations comparing with the synthetics of our mechanism and the Harvard CMT solution. We can see that because of the difference in strike in the two mechanisms, there is a big difference between the SH displacements of the two synthetics. The Harvard solution predicts nearly nodal SH displacements with negative polarity at most KNET stations, which is contradictory to the positive SH displacement of the observations. Our solution fits the three-component data quite well.

One of the best recorded shallow events is the magnitude 5.1 earthquake (event 328) which occurred at about an equal distance between the two arrays. Figure 4 displays the observations and synthetics. The overall fit is excellent in both shapes and amplitudes. Note that the SV and SH surface waves (Love and Rayleigh) are about equal in amplitude, indicating a mixed mechanism.

Although our focal mechanism is very similar to the Harvard CMT solution (see Table 3), the focal depth (15 km) is distinctly shallower than the depth of the latter (44 km). Because we have the advantage of using regional waveform data, the source depth is better constrained, mostly by the relative strengths of *Pnl* to surface waves. The sensitivity of focal depth to the *Pnl*/surface wave ratio can be seen in Figure 5 where the synthetics as a function of depth are displayed for the vertical component of station SBRA. This particular station shows anomalous surface wave amplitudes

Table 3. Source Mechanisms and Depths of Events From the Waveform Inversion

Event	Strike	Dip	Rake	M_w	h, km
276	320°	70°	-30°	4.4	150
	320°	70°	-50°	4.5	150
289a	330°	60°	-60°	3.9	5
	320°	80°	-30°	4.0	5
289b	60°	50°	30°	4.2	160
	50°	70°	40°	4.2	160
307	210°	50°	60°	4.7	150
	210°	50°	60°	4.8	150
311a	270°	40°	60°	4.7	15
	270°	40°	30°	4.8	15
	322°	25°	111°	5.0	19
311b	0°	40°	40°	4.2	10
	0°	50°	40°	4.2	15
313	10°	30°	60°	4.5	15
	0°	30°	40°	4.6	20
317	40°	70°	80°	5.5	190
	50°	70°	80°	5.5	180
	33°	77°	71°	5.6	188
322	30°	50°	-90°	4.7	10
	20°	50°	-90°	4.7	10
	29°	60°	-75°	5.1	33
328	180°	40°	-60°	5.1	15
	180°	40°	-60°	5.1	10
	211°	33°	-49°	5.6	44
339	60°	60°	-80°	5.5	110
	50°	70°	-90°	5.6	110
	57°	74°	-85°	5.7	131
341	300°	40°	-20°	4.9	100
	300°	30°	-20°	5.0	100

For each event the first line is the result using the two arrays, and the second line is the result using two stations, SBRA and AAK. The Harvard centroid moment tensor (CMT) solution, if available, is listed in the third line.

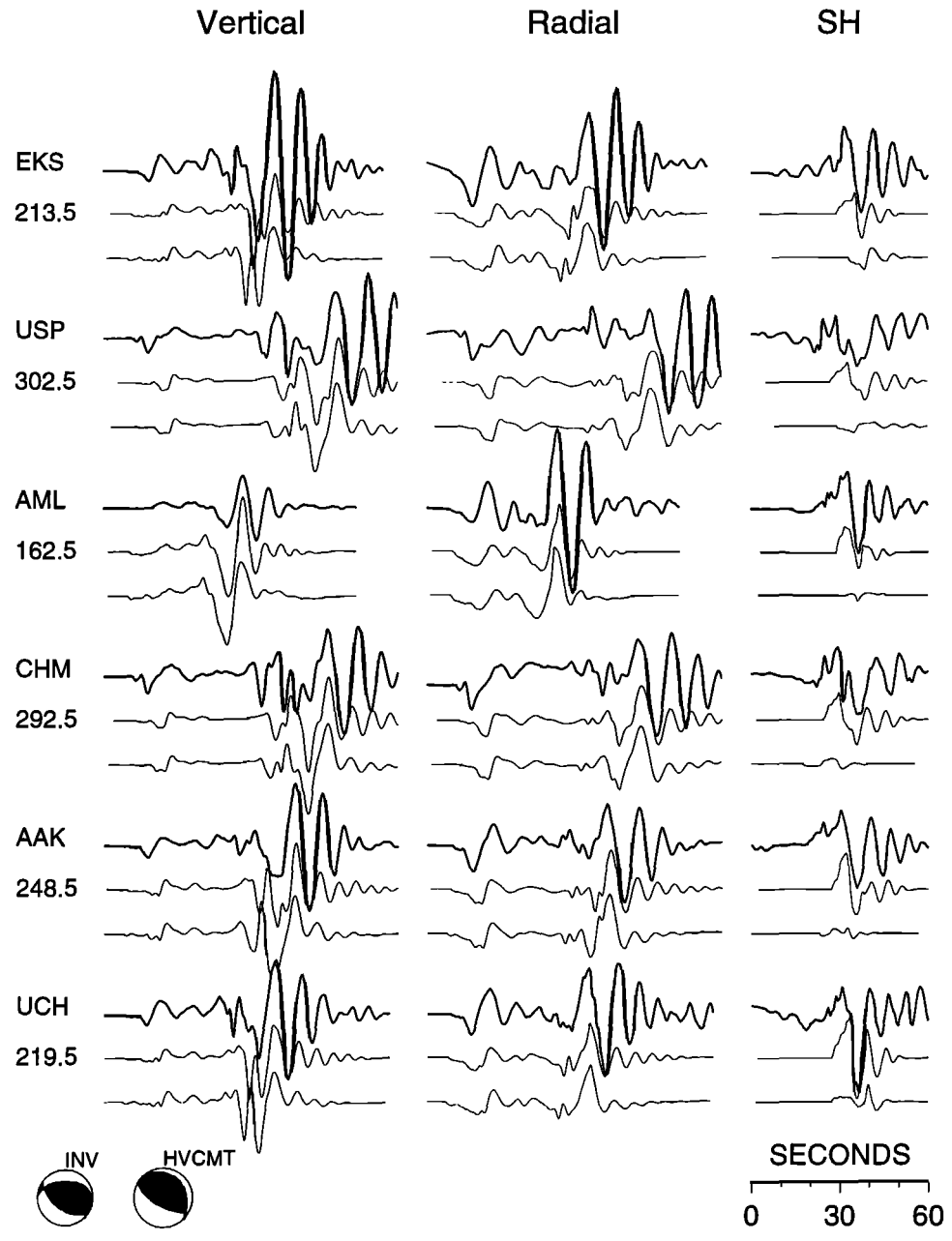

Figure 3. Comparison of the KNET observed waveforms (heavy traces) of event 311a with the synthetics of our source mechanism (middle traces) and the Harvard centroid moment tensor (CMT) solution (bottom traces). Both data and synthetics are plotted in true amplitude with the distance scaling applied ($p = 0.5$). Numbers below station names are the distance ranges in kilometers. The stations are ordered according to their azimuths with respect to the source. Note the difference of the two SH synthetics.

relative to the PAKH array, as can be seen in Figure 4 (see the Rayleigh waves of SBRA in the figure; SH is close to nodal for SBRA). Similar patterns are observed for most other events at this station. One possible cause is the presence of unconsolidated sedimentary material beneath the site since it was located in the Peshawar basin (see Plate 1). A sediment wedge is also a possible cause of the distorted Pnl, as shown in Figure 5. Even with these complications, the ratio of Pnl to Rayleigh forces the relatively shallow depth estimate.

Figure 6 presents the waveform misfit error as a function of source depth. It shows a well-defined minimum at 15 to 20 km for this event. For all crustal events our solutions prefer shallower depths than the ISC depths or Harvard CMT solutions when the latter exists (Table 3). We will discuss this in more detail later.

For intermediate-depth earthquakes, the waveforms become simpler with sharp P arrivals and an absence of surface waves. Figure 7 shows an example comparison of synthetics and observed waveforms for one of

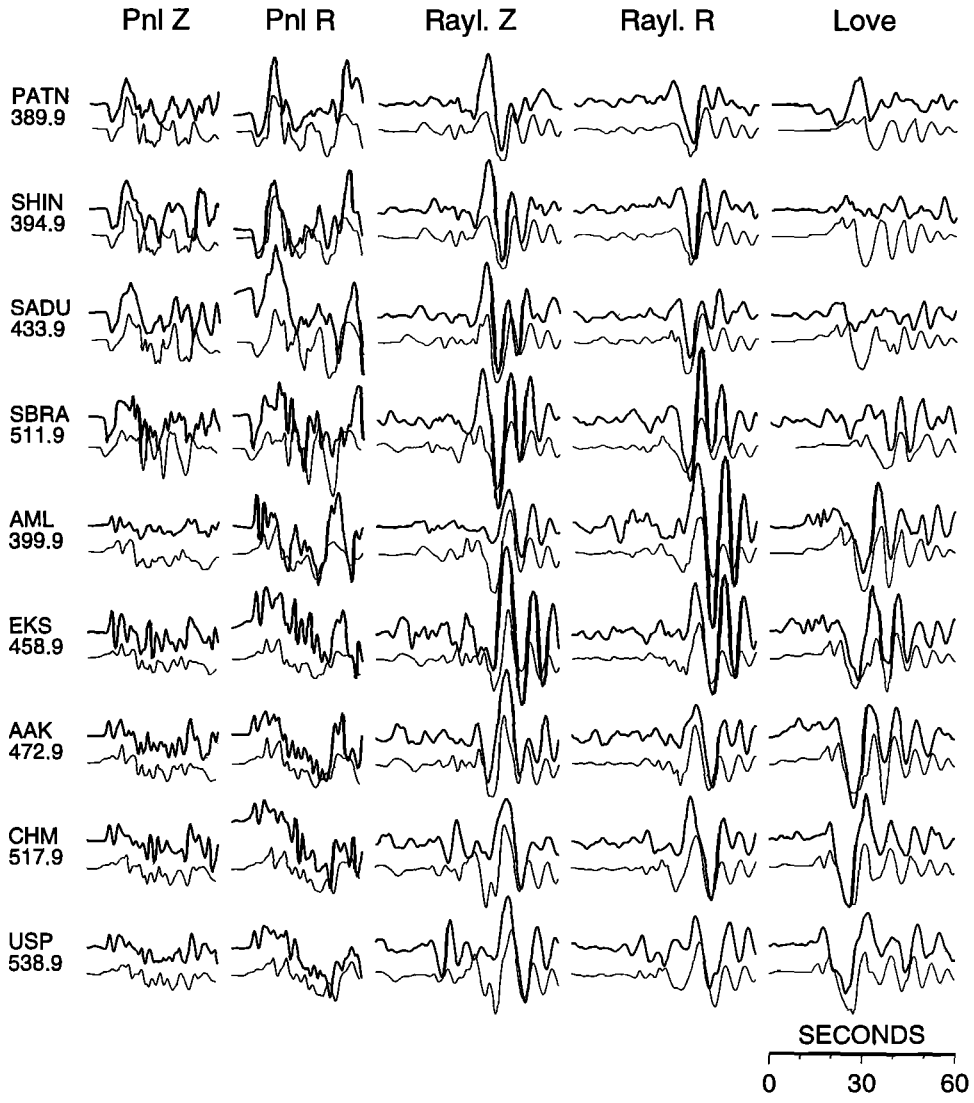

Figure 4. Waveform fit for event 328; heavy lines are the data. Both the data and the synthetics are plotted in true amplitude with the distance scaling applied ($p = 1$ for Pnl, and $p = 0.5$ for surface waves). Numbers under station names are the distance ranges in kilometers.

the mantle events (event 341, depth 122 km). An easily recognizable phase is the large-amplitude, long-period phase (labeled as sPn) before the direct S arrival. It is actually produced by the S-to-P conversion at the free surface and then reflected to the receiver by the Moho ($sPmP$). After the reflection reaches the critical angle, part of this P wave travels along the Moho as a head wave (sPn), which has a similar apparent velocity to the direct P. These shear-coupled P waves ($sPmP + sPn$) at regional distances from intermediate-depth earthquakes have been noted earlier by *Zhao and Helmberger* [1993]. Recently, they have been reported in many places [*Singh et al.*, 1995; *Langston*, 1996; *Zandt et al.*, 1996]. Our data show that they are commonly observed in the Pamir-Hindu Kush region. Because of the strong amplitude of this phase and small move-out with distance with respect to the direct P, the time separation between P and sPn is ideal for controlling focal depth.

Because of the cut-and-paste nature of our source estimation technique, the time separation between P and sPn waves is not employed to constrain depth. This causes no difficulty in inverting for depths of crustal events because their depths are mainly controlled by the amplitude of surface waves. Since the time separation between P and sPn is so important for depth determination of mantle events, we perform the inversion in two steps. First, the seismogram is broken down into P and S segments and inverted for source mechanism and a rough estimation of depth. Then we fix the source mechanism at the "best" mechanism and use the whole waveform to search for a more precise focal depth, controlled by the sPn-P separation. The misfit errors as a function of depth for the mantle events are also presented in Figure 6. It can be seen that most deep events show good depth resolution and are quite consistent with the ISC bulletin and the Harvard CMT depths.

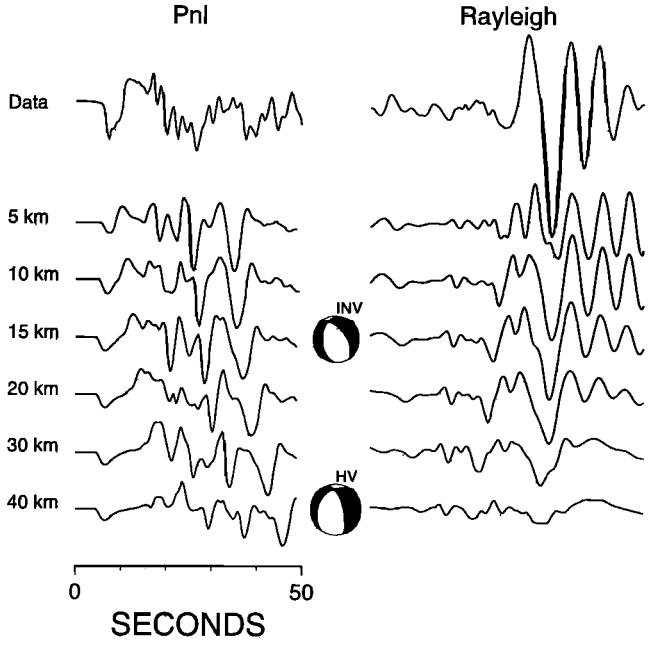

Figure 5. Vertical displacement of event 328 at station SBRA and the corresponding synthetics for different source depths. The best depth estimate is at 15 km. The bottom traces represent the synthetics of the Harvard CMT solution (source depth 44 km).

5. Event Relocation

After source depths are established from the waveform inversion we can relocate events horizontally using their first-arrival times. By fixing the source depth the strong trade-off between the depth and origin time of event can be avoided. The relocation is also done using a grid search method where we minimize the object function defined by

$$\Phi(x,y) = \sqrt{\frac{1}{N}\sum_{i=1}^{N}(\delta T_i - \overline{\delta T})^2} + \lambda \Delta r, \qquad (1)$$

here x and y are horizontal coordinates and δT_i is the travel time residual of the first-arrival at station i. The average residual over all stations $\overline{\delta T}$ is subtracted to remove the uncertainty of origin time. Δr is the offset between the new location and the original location. Note that our station distribution can only provide good control of an event's location in the north-south direction (see Plate 1). Because all travel time residuals are de-meaned, the Δr term in the above formula is needed to force a local minimum around the original location. The weighting constant λ is set to 0.01 s km^{-1} for this study. If good station coverage is available, this parameter can be chosen smaller to allow more freedom in the relocation.

For each event an area of 1° by 1° centered at its ISC location is grid searched. The relocation results are listed in Table 4. It can be seen that for all deep events and large shallow events ($m_b \geq 5$) the differences between the ISC locations and the new locations are less than 10 km. However, there can be up to 30 km of offset for small shallow events (see events 289a and 311b). This is not surprising because deep events and larger shallow events usually have sharp onsets at teleseismic distances which can be easily picked. However, small shallow events often show emergent onsets, and the time-picking errors can be relatively large.

The largest relocation difference (31 km) occurs for event 289a, which is the smallest (M_w 3.9) among the 12 events. Before the relocation it shows consistently early P arrivals (δT of more than -4 s) at the PAKH array and late P arrivals (δT of +3 s) at the KNET. As a result of relocation, the event is moved from the southern slope of the Trans-Alai Range to the northern foothills (Figure 8). This offset is mostly in the north-south direction, so it is quite reliable. Moreover, our relocation appears to be quite acceptable at this new location. That is, there is ample evidence of Quaternary and Holocene faulting and folding along the northern margin of the Trans-Alai Range [*Nikonov*, 1988; *Burtman and Molnar*, 1993; *Strecker et al.*, 1995]. Of course, a more direct proof would be comparing it with a re-

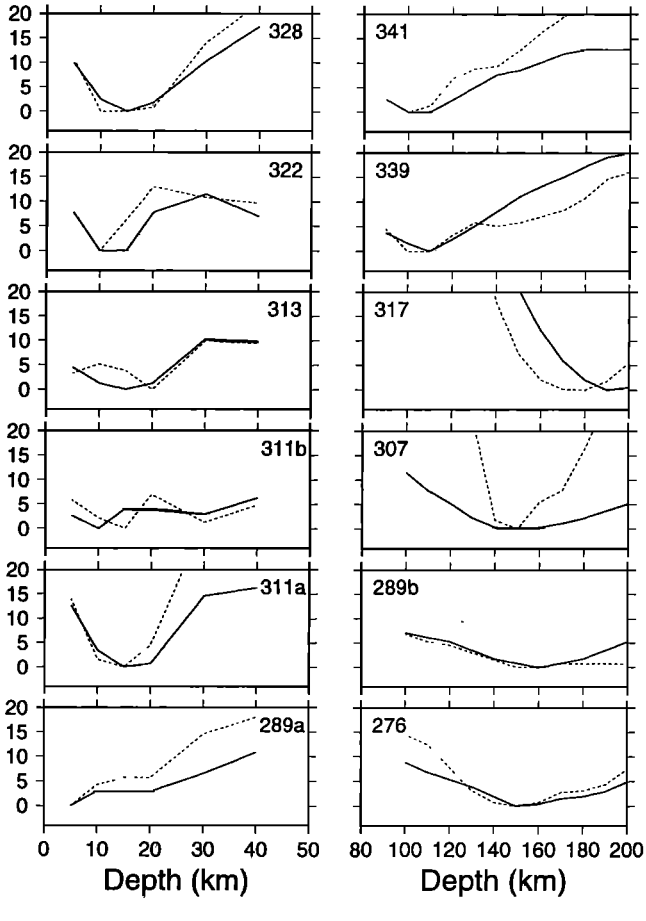

Figure 6. Waveform misfit error as a function of depth. Solid lines are results from the two-array inversion; dashed lines are from the two-station inversion. The misfit errors for each event are given in percentages as normalized by the minimum value.

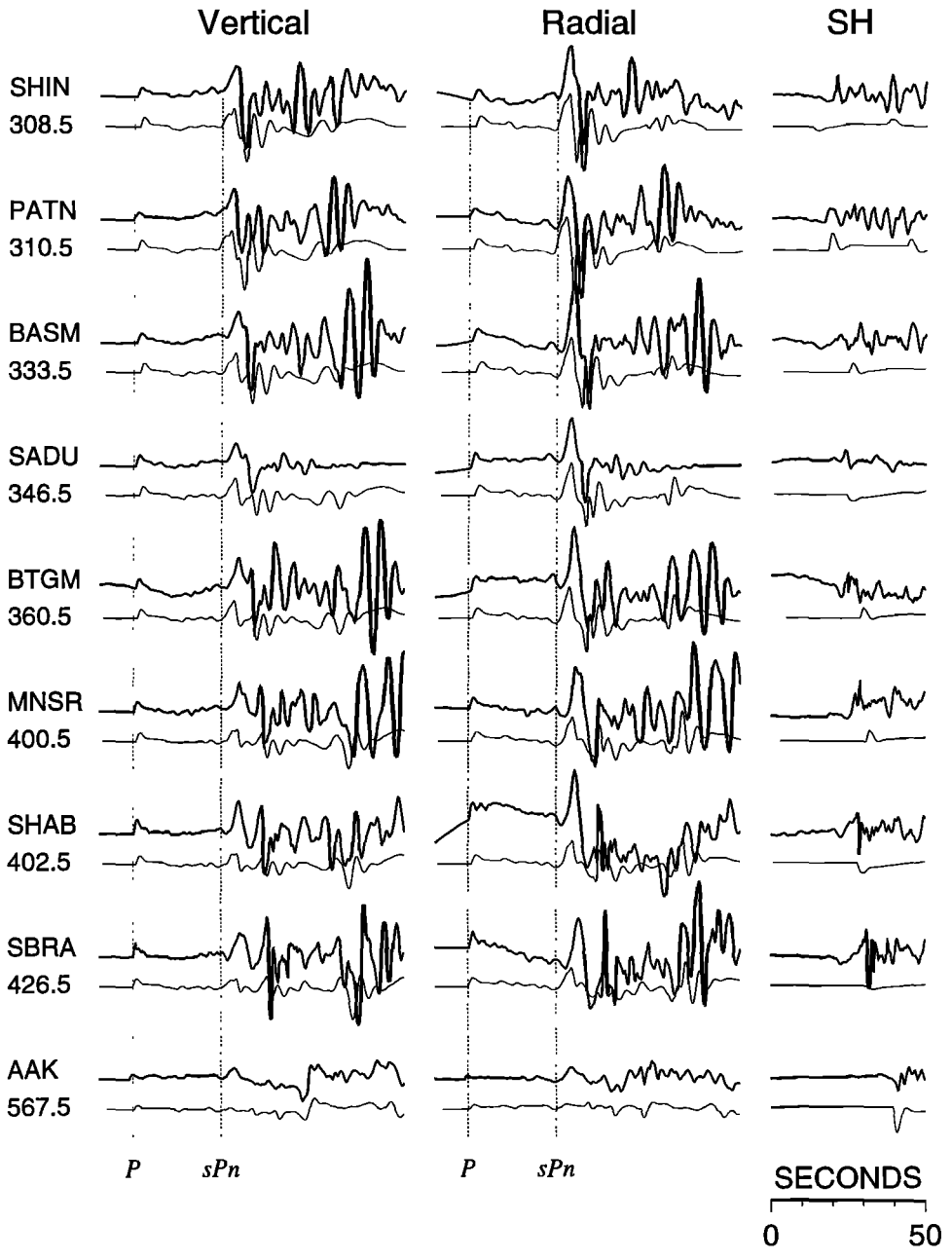

Figure 7. Waveform fit for mantle event 341; heavy lines are the data. Both the data and the synthetics are plotted in true amplitude with the distance scaling applied ($p = 1$). Numbers under station names are the distance ranges in kilometers. Two parallel dashed lines show the arrivals of the direct P and the sPn.

gional catalog. Unfortunately, it is not available to us for this time period.

6. Lateral Variation of Shallow Structure

Most propagation paths from our events to the KNET and PAKH arrays traverse more than one major tectonic block. These complications did not disrupt our waveform modeling success using the CAP approach which allows some time shifting between observations and synthetics for both surface waves and Pnl. Generally, Pnl is more stable than the surface waves which are easily affected by shallow structure. A by-product of our source inversion is the time shift between the observed waveform and the 1-D synthetics. This value can be used to map out the lateral variation with respect to the 1-D velocity model. Plate 2 shows the velocity anomalies of Love waves as measured by the time shifts of SH components. Red and yellow paths indicate lower velocities than the 1-D model, and blue and green paths indicate faster velocities. We can see that the Love waves are faster for paths within the Pamir plateau and Hindu Kush Range, while paths associated

Table 4. Relocation Result by Fixing Source Depth and Using First-Arrival Times

Event	Latitude	Longitude	Δr^a	Δt_0^b, s
276	38.10N	73.12E	2	-0.41
	38.08N	73.20E	7	-0.62
289a	39.50N	72.94E	31	0.26
	39.50N	72.86E	29	0.30
289b	38.24N	74.40E	6	0.36
	38.22N	74.44E	2	0.29
307	37.34N	72.06E	7	-0.16
	37.34N	72.06E	7	-0.28
311a	41.03N	72.42E	9	1.75
	40.99N	72.50E	11	1.12
311b	34.71N	69.17E	18	4.00
	34.65N	69.25E	26	2.90
313	38.62N	69.80E	9	0.93
	38.56N	69.84E	16	0.42
317	36.57N	70.85E	13	0.76
	36.57N	70.93E	14	0.06
322	33.97N	67.45E	17	4.35
	33.91N	67.49E	10	4.16
328	38.63N	72.63E	7	3.16
	38.63N	72.59E	8	3.05
339	37.87N	72.17E	10	0.17
	37.83N	72.25E	6	-0.04
341	37.85N	72.19E	7	0.58
	37.87N	72.13E	10	0.53

For each event the first line is the result using the two arrays and the second line is the result using two stations, SBRA and AAK.

[a]Offset in kilometers between new locations and the ISC locations.

[b]Difference in origin time of event from the ISC bulletin. Positive value means that the new origin time is earlier.

with the Tien Shan or traversing the Ferghana and Peshawar basins are slower. There are also complications to this simple pattern. Paths from events 289a and 328 to the KNET display contradictory anomalies which seem difficult to interpret. However, as we have shown before, event 289a is very shallow and located at the southern edge of the Alai Valley (Figure 8), so the Love waves going north are strongly influenced by the low-velocity sedimentary valley. On the other hand, event 328 is deeper (15-20 km) under the mountainous Pamir, and the propagation is less affected by shallow heterogeneities. A numerical sensitivity test shows that travel times of surface waves at these ranges are mainly controlled by the S velocities above the source depth [*Song et al.*, 1996].

7. Results From Two Stations

Both KNET and PAKH are relatively small aperture arrays with respect to events in the Pamir-Hindu Kush region. The successful source retrieval and relocation from these two arrays suggest that it is also possible to accomplish the same task by using only two stations, one from each array. This is of great practical significance as a new IRIS station, NIL, was installed near the temporary station SBRA in 1993 (Plate 1). In addition, one of the KNET stations, AAK, is also occupied as a permanent IRIS station. If we can calibrate the propagation paths to stations AAK and SBRA using our 12 events, we will be able to process events in this region routinely in the future, assuming that NIL will perform similarly to SBRA.

Several studies demonstrate that a single, three-component broadband station is adequate for retrieving the source mechanism of events at regional distances, provided that the velocity structure along the ray path and the event location are known reasonably well [*Fan and Wallace*, 1991; *Zhao and Helmberger*, 1993; *Dreger and Helmberger*, 1993; *Walter*, 1993]. This is because the amplitude ratio between SV and SH is quite sensitive to the source orientation [*Langston*, 1982]. In unfavorable situations, adding one more station, even with a small aperture, can greatly reduce the nonuniqueness of solution [*Dreger and Helmberger*, 1993]. Because of the relaxation of timing in our source inversion technique, as discussed earlier, event mislocation and use of an inappropriate velocity model should not be a major problem. However, using two stations will help stabilize the inversion for small events with low signal-to-noise ratios.

As a test, we repeat the same waveform inversion and relocation procedure above but using only stations AAK and SBRA. Note that these two stations actually give a maximum aperture for events in the Pamir-Hindu Kush

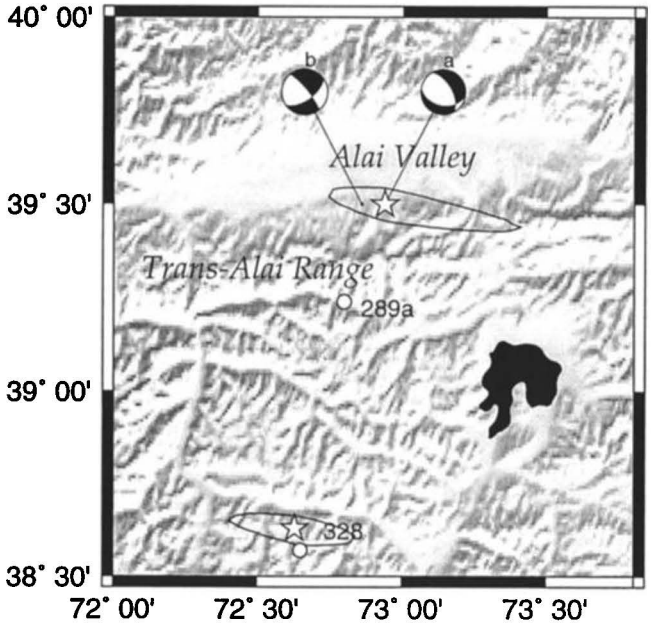

Figure 8. Comparison of locations of the ISC epicenters (circles) and the relocation (stars) for events 289a and 328. Relocation uncertainty is given by the 0.8 s contour of the object function (see text). The source mechanisms of event 289a from the two-array inversion (a) and the two-station inversion (b) are also shown.

region. The source mechanisms and relocation results are summarized in Tables 3 and 4. A comparison of depths determined by the two-array inversion and the two-station inversion is presented in Figure 6. Quite encouragingly, the two-station inversion gives very similar results to the two-array inversion. For most events the difference in strike, dip, and rake of source mechanisms are within 10° and the relocations are very close (see Table 4).

It is interesting to see that two stations with only two arrival times can be used to relocate earthquakes, which have four unknowns involved (location plus origin time of event). Part of the reason is that the source depth is determined independently from waveforms, which reduces the number of unknowns to three. The origin time is further removed by de-meaning travel time residuals. But this introduces the problem that we are unable control the event's location in the east-west direction, given the current station distribution. So, our relocations are most reliable only for the north-south component. One way to solve this problem is by using one more station, either in the east or west of the region. Or one can use both P and S arrivals. But the latter are usually difficult to pick [see *Saikia et al.*, 1996].

8. Discussion

A comparison of our results with the ISC catalog shows that the focal depths for the mantle events are compatible, but they can differ by as much as 30 km for the crustal events. This is not surprising because the ISC catalog relies heavily on the determination of depth phases (pP, etc.) to establish focal depth. However, identifying depth phases on short period recordings can be very difficult, if not impossible, for crustal events. This is because the source time functions of crustal events are often complicated and the separations between depth phases and the first-arrivals are small. Without a reliable depth phase constraint, a strong trade-off exists between the origin time and depth. *Zhao and Helmberger* [1991], using long period teleseismic body waveforms, found that throughout the Tibetan plateau the PDE-reported crustal events are systematically located about 15 km deeper and occurred about 4 s earlier than the relocation results. An advantage of using regional broadband waveforms is that focal depths can be better constrained, either from amplitude ratio of *Pnl* to surface waves for crustal events or from the time separation between the direct P and depth phase sPn for mantle events. In this region we find that all crustal events are relocated shallower than quoted in the ISC bulletin or the Harvard CMT solutions. It is generally believed that the middle to lower part of the continental crust is weak and mostly deformed aseismically [*Chen and Molnar*, 1983]. We suspect that the clustering of earthquakes around 50 km depth in Figure 1 might be due to mislocations. Most of them will probably, after relocation, move to either the upper crust or the uppermost mantle.

As magnitudes of shallow events drop below about 4.5, the number of useful teleseismic recordings becomes small and locating events becomes progressively more difficult. However, accurate location of these shallow events is important for seismotectonic studies as well as for the nuclear explosion monitoring. In this study we have established a procedure of focal mechanism determination and relocation using as few as two broadband stations at regional distances. Besides the potential capability of providing a more uniform and well-constrained data set of source mechanisms and depths for the Pamir-Hindu Kush region, our technique can also be very useful for the International Monitoring System (IMS). Currently, the IMS is issuing event bulletins on a daily basis. Under such a time frame, only data from a few digital stations are available. This requires extracting as much information from the waveform data as possible. A real-time event location program by a single three-component station is under development, which can provide preliminary location within minutes of an event's occurrence. Our procedure can then be employed to refine the location, independent of the PDE or ISC locations, which usually come weeks or months later.

The source mechanisms of crustal events that we obtained are generally consistent with the regional tectonics and show some correlation with the topography (Plate 1). Events at low elevations show predominant thrusting mechanisms (see events 311a, 311b, and 313), while at high elevations, normal-faulting events are observed (event 322 and 328). This pattern was found in the Pamir region [*Strecker et al.*, 1995] and the adjacent Tibet plateau [*Molnar and Lyon-Caen*, 1989]. The existence of normal faulting in a continental collision environment may simply result from the high potential energy of thickened crust and gravitational instability [*Molnar and Lyon-Caen*, 1989; *Strecker et al.*, 1995]. The large normal-faulting component in the source mechanism of event 289a is more or less unexpected (Figure 8). Most Harvard CMT solutions for events along the Trans-Alai mountain front have thrusting mechanisms. As we mentioned before, event 289a is the smallest event so the signal-to-noise ratio of waveforms is low. However, we have tested the possibility of thrust faulting for this event by forward modeling. It turned out that thrust-faulting mechanisms could not even fit the polarities of *Pnl* waveforms, thus they can be ruled out.

The source mechanisms of the intermediate-depth events are, perhaps, the most interesting. All these events show either thrusting or normal-faulting mechanisms and the strikes of the fault planes essentially follow the strike of the Wadati-Benioff zone (Plate 1). Out of the six intermediate-depth events, three shallower ones (events 276b, 339, and 341, all with depths less than 150 km) have P axes nearly vertically oriented, indicating a down dip compression in the Wadati-Benioff zone. The other three (events 289b, 307 and 317, deeper than 150 km), however, show vertical T axes, thus in-

dicating a down dip extension. Whether this is a general pattern for the intermediate-depth events in this region is not clear because of the very limited number of our events. Previous studies have shown that earthquakes below 170 km have consistent vertically oriented T axes, while above 170 km the orientations are more scattered [*Billington et al.*, 1977; *Roecker et al.*, 1980; *Chatelain et al.*, 1980]. The prevalence of down dip tension in the vertically oriented section of the Wadati-Benioff zone suggests that the deformation in this part is mostly internal and results from body forces acting on relatively dense material [*Roecker et al.*, 1980]. This is supported by the existence of a high-velocity anomaly below 200 km near the Hindu Kush seismic zone [*Mellors et al.*, 1995]. Combining with the observation of a seismicity gap and a sudden change of dip angle of the Wadati-Benioff zone around a depth of 170 km (Figure 1), it seems that the deeper, vertically oriented seismic zone represents a segment of slab that detached from the segment above and is sinking into the mantle under its own weight. Another explanation is that this part is an oceanic slab subducted prior to the collision [*Chatelain et al.*, 1980]. Since the oceanic subduction in this region ended at least 40 myr. ago [*Molnar and Tapponnier*, 1975; *Tapponnier et al.*, 1981], how this slab survives such a long time at this depth is an open question. Using regional travel time data, *Roecker* [1982] showed that there is a low-velocity anomaly associated with the Hindu Kush seismic zone between depth ranges of 35 to 150 km. He interpreted this part as a portion of continental crust subducted during the collision. In order to resolve the actual geometry of the slabs and their relationship to the shallow geology, more data are needed.

Acknowledgments. We thank M. W. Hamburger and two anonymous referees for their constructive criticism and comments which helped us to improve the manuscript substantially. Seismic data from the Pakistan Experiment were collected in a collaborative effort between the Pakistan Government, New Mexico State University, and Rensselaer Polytechnic Institute. We also thank the IRIS Data Center for providing KNET data. This work has been supported by ARPA contract F19628-95-C-0093 at Woodward-Clyde Federal Services and by the Department of Defense as monitored by the Air Force Office of Scientific Research under contract F19628-95-C-0096 at Caltech. Contribution 5735, Division of Geological and Planetary Sciences, California Institute of Technology, Pasadena, California.

References

Beloussov, V. V., et al., Structure of the lithosphere along the deep seismic sounding profile: Tien Shan–Pmairs–Karakorum–Himalayas, *Tectonophysics*, *70*, 193–221, 1980.

Billington, S., B. L. Isacks, and M. Barazangi, Spatial distribution and focal mechanisms of mantle earthquakes in the Hindu Kush-Pamir region: A contorted benioff zone, *Geology*, *5*, 699–704, 1977.

Burtman, V. S., and P. Molnar, Geological and geophysical evidence for deep subduction of continental crust beneath the Pamir, *Geol. Soc. of Am., Spec. Pap.*, *281*, 1993.

Chatelain, J. L., S. W. Roecker, D. Hatzfeld, and P. Molnar, Microearthquake seismicity and fault plane solutions in the Hindu Kush region and their tectonic implications, *J. Geophys. Res.*, *85*, 1365–1387, 1980.

Chen, W. P., and P. Molnar, Focal depths of intracontinental and intraplate earthquakes and their implications for the thermal and mechanical properties of the lithosphere, *J. Geophys. Res.*, *88*, 4183–4214, 1983.

Dreger, D. S., and D. V. Helmberger, Determination of source parameters at regional distances with three-component sparse network data, *J. Geophys. Res.*, *98*, 8107–8125, 1993.

Dziewonski, A. M., and J. H. Woodhouse, An experiment in systematic study of global seismicity: Centroid-moment tensor solutions for 201 moderate and large earthquakes of 1981, *J. Geophys. Res.*, *88*, 3247–3271, 1983.

Fan, G. W., and T. C. Wallace, The determination of source parameters for small earthquakes from a single very broadband seismic station, *Geophys. Res. Lett.*, *18*, 1385–1388, 1991.

Fan, G., J. F. Ni, and T. C. Wallace, Active tectonics of the Pamirs and Karakorum, *J. Geophys. Res.*, *99*, 7131–7160, 1994.

Hamburger, M. W., D. R. Sarewitz, T. L. Pavlis, and G. A. Popandopulu, Structural and seimic evidence for intracontinental subduction in Peter the first Range, Central-Asia, *Geol. Soc. Am. Bull.*, *104*, 397–408, 1992.

Harvey, D., Comparative seismic detection and location capabilities of IRIS and GSETT-3 stations within central Asia, *IRIS Newsletter*, *XV*, 5–7, 1996.

Helmberger, D. V., and G. R. Engen, Modeling the long-period body waves from shallow earthquakes at regional ranges, *Bull. Seismol. Soc. Am.*, *70*, 1699–1714, 1980.

Kawakatsu, H., Automatic near-realtime CMT inversion, *Geophys. Res. Lett.*, *22*, 2569–2572, 1995.

Langston, C. A., Single-station fault plane solutions, *Bull. Seismol. Soc. Am.*, *72*, 729–744, 1982.

Langston, C. A., The SsPmp phase in regional wave propagation, *Bull. Seismol. Soc. Am.*, *86*, 133–143, 1996.

Mellors, R. J., G. L. Pavlis, M. W. Hamburger, H. J. Al-Shukri, and A. A. Lukk, Evidence for a high-velocity slab associated with the Hindu Kush seismic zone, *J. Geophys. Res.*, *100*, 4067–4078, 1995.

Molnar, P., and H. Lyon-Caen, Fault plane solutions of earthquakes and active tectonics of the Tibetan plateau and its margins, *Geophys. J. Int.*, *99*, 123–153, 1989.

Molnar, P., and P. Tapponnier, Cenozoic tectonics of Asia: Effects of a collision, *Science*, *189*, 419–426, 1975.

Nikonov, A. A., Reconstruction of the main parameters of old large earthquakes in Soviet Central Asia using the paleoseismogeological method, *Tectonophysics*, *147*, 297–312, 1988.

Polet, J., and H. Kanamori, Automated CMT inversion using surface waves (abstract), *Eos, Trans. AGU*, *77(46)*, Fall Meeting Suppl., 1995.

Roecker, S. W., Velocity structure of the Pamir-Hindu Kush region: Possible evidence of subducted crust, *J. Geophys. Res.*, *87*, 945–959, 1982.

Roecker, S. W., O. V. Soboleva, I. L. Nersesov, A. A. Lukk, D. Hatzfeld, J. L. Chatelain, and P. Molnar, Seismicity and fault plane solutions of intermediate depth earthquakes in the Pamir-Hindu Kush region, *J. Geophys. Res.*, *85*, 1358–1364, 1980.

Saikia, C. K., Modified frequency-wavenumber algorithm for regional seismograms using filon-quadrature method – Modeling of Lg waves in eastern North-America, *Geophys. J. Int.*, *118*, 142–158, 1994.

Saikia, C. K., B. B. Woods, L. Zhu, H. K. Thio, and D. V. Helmberger, Path calibration, source estimation and regional discrimination for the Middle East: Application

to the Hindu-Kush region, *Tech. Rep. PL-TR-96-2069*, Phillips Lab., Hanscom AFB, Mass., 1996.

Sandvol, E., J. Ni, and T. Hearns, Seismic azimuthal anisotropy beneath the Pakistan Himalaya, *Geophys. Res. Lett.*, *21*, 1635–1638, 1994.

Singh, S. K., M. Santoyo, and J. Pacheco, Intermediate-depth earthquakes in central mexico: Implications for plate waves, *Geophys. Res. Lett.*, *22*, 527–530, 1995.

Sipkin, S. A., Estimation of earthquake source parameters by the inversion of waveform data: Global seismicity, 1981-1993, *Bull. Seismol. Soc. Am.*, *76*, 1515–1541, 1986.

Song, X. J., D. V. Helmberger, and L. Zhao, Broad-band modeling of regional seismograms: The Basin and Range crustal structure, *Geophys. J. Int.*, *125*, 15–29, 1996.

Strecker, M. R., W. Frisch, M. W. Hamburger, L. Ratschbacher, S. Semiletkin, A. Zamoruyev, and N. Sturchio, Quaternary deformation in the Eastern Pamirs, Tadzhikistan and Kyrgyzstan, *Tectonics*, *14*, 1061–1079, 1995.

Tapponnier, P., M. Mattauer, F. Proust, and C. Cassaigneau, Messozoic ophiolites, sutures, and large-scale tectonic movements in Afghanistan, *Earth Planet. Sci. Lett.*, *52*, 355–372, 1981.

Walter, W. R., Source parameters of the June 29 Little Skull Mountain earthquake from complete regional waveforms at a single station, *Geophys. Res. Lett.*, *20*, 403–406, 1993.

Wang, C. Y., and R. B. Herrmann, A numerical study of P, SV, and SH-wave generation in a plane layered medium, *Bull. Seismol. Soc. Am.*, *70*, 1015–1036, 1980.

Zandt, G., S. L. Beck, S. R. Ruppert, C. J. Ammon, D. Rock, E. Minaya, T. C. Wallace, and P. G. Silver, Anomalous crust of the Bolivian Altiplano, central Andes: Constraints from broadband regional seismic waveforms, *Geophys. Res. Lett.*, *23*, 1159–1162, 1996.

Zhao, L. S., and D. V. Helmberger, Geophysical implication from relocation of Tibetan earthquakes; Hot lithosphere, *Geophys. Res. Lett.*, *18*, 1070–1084, 1991.

Zhao, L. S., and D. V. Helmberger, Source retrieval from broadband regional seismograms: Hindu Kush region, *Phys. Earth Planet. Inter.*, *78*, 69–95, 1993.

Zhao, L. S., and D. V. Helmberger, Source estimation from broadband regional seismograms, *Bull. Seismol. Soc. Am.*, *84*, 91–104, 1994.

Zhu, L., and D. V. Helmberger, Regional earthquake waveform modeling on the Tibetan plateau, in *Proceedings of the 16th Annual Seismic Research Symposium*, edited by J. J. Cipar, J. F. Lewkowicz, and J. M. McPhetres, vol. PL-TR-94-2217, pp. 407–413, Phillips Lab., Hanscom AFB, Mass., 1994.

Zhu, L., and D. V. Helmberger, Intermediate depth earthquakes beneath the India-Tibet collision zone, *Geophys. Res. Lett.*, *23*, 435–438, 1996a.

Zhu, L., and D. V. Helmberger, Advancement in source estimation techniques using broadband regional seismograms, *Bull. Seismol. Soc. Am.*, *86*, 1634–1641, 1996b.

Zhu, L., R. S. Zeng, F. T. Wu, T. J. Owens, and G. E. Randall, Preliminary study of crust-upper mantle structure of the Tibetan plateau by using broadband teleseismic body waveforms, *Acta Seismol. Sinica*, *6*, 305–315, 1993.

D. V. Helmberger and L. Zhu, Seismological Laboratory, California Institute of Technology, Pasadena, CA 91125. (e-mail: lupei@gps.caltech.edu)

C. K. Saikia and B. B. Woods, Woodward-Clyde Federal Services, 566 El Dorado Street, Pasadena, CA 91101.

(Received October 24, 1996; revised June 12, 1997; accepted June 20, 1997.)